Crystallographic and Magnetic Properties of the Spinel-type Ferrites $Zn_xCo_{1-x}Fe_2O_4$ ($0.0 \leq x \leq 0.75$)

A. K. Azad[a] , A. K. M. Zakaria[b], Md. Yusuf Jewel[c], Abu Saeed Khan[c], S. M. Yunus[b], I. Kamal[b], T. K. Datta[b] and S.–G. Eriksson[d]

[a]*Faculty of Integrated Technologies, Universiti Brunei Darussalam, Gadong BE 1410, Brunei Darussalam*
[b]*Institute of Nuclear Science and Technology, Bangladesh Atomic Energy Commission, Savar, Dhaka, Bangladesh*
[c]*Department of Physics, Jahangirnagar University, Savar, Dhaka, Bangladesh*
[d]*Department of Chemical & Biological Engineering, Chalmers University of Technology, Gothenburg, Sweden*

Abstract. Ultrahigh frequencies (UHF) have applications in signal and power electronics to minimize product sizes, increase production quantity and lower manufacturing cost. In the UHF range of 300 MHz to 3 GHz, ferrimagnetic iron oxides (ferrites) are especially useful because they combine the properties of a magnetic material with that of an electrical insulator. Ferrites have much higher electrical resistivity than metallic ferromagnetic materials, resulting in minimization of the eddy current losses, and total penetration of the electromagnetic (EM) field. Hence ferrites are frequently applied as circuit elements, magnetic storage media like read/write heads, phase shifters and Faraday rotators. The electromagnetic properties of ferrites are affected by operating conditions such as field strength, temperature and frequency. The spinel system $Zn_xCo_{1-x}Fe_2O_4$ (x=0.0, 0.25, 0.50 and 0.75) has been prepared by the standard solid state sintering method. X-ray and neutron powder diffraction measurements were performed at room temperature. Neutron diffraction data analysis confirms the cubic symmetry corresponding to the space group Fd3m. The distribution of three cations Zn^{2+}, Co^{2+} and Fe^{3+} over the spinel lattice and other crystallographic parameters like lattice constant, oxygen position parameter, overall temperature factor and occupancies of different ions in different lattice sites for the samples have been determined from the analysis of neutron diffraction data. The lattice constant increases with increasing Zn content in the system. The magnetic structure was found to be ferrimagnetic for the samples with $x \leq 0.50$. Magnetization measurements show that with the increase of Zn content in the system the value of saturation magnetization first increases and then decreases. The variation of the magnetic moment with Zn substitution has been discussed in terms of the distribution of magnetic and non-magnetic ions over the A and B sub-lattices and their exchange coupling.

Keywords: Ferrites; neutron diffraction; structural characterization; magnetic measurements.
PACS: 61.05Cp; 61.05Fm; 75.47Lx; 75.50Gg

INTRODUCTION

Ferrites have got wide spread applications in different fields for its wide variety of magnetic characteristics [1-2]. Among the applications, ferrites are used in microwave operations, analog devices, transformer cores, high quality filters and radio frequency circuits [3-10]. Ferrites are considered one of the very important magnetic materials used in low, high and very high frequency circuits. More recently, much interest have been paid in studying ferrites of varying compositions by using different techniques [11-15]. The general chemical formula for the spinel type ferrites is AB_2O_4, where A and B represent divalent and trivalent metal ions (cations), respectively and O represents the oxygen ions. The spinel structure consists of a face-centered cubic lattice of oxygen ions with two types of interstitial holes for cations of tetrahedral (A) and octahedral (B) site symmetries. Cations preferentially occupy these two sites depending on their relative size and the criteria of the minimization of the total crystal energy of the system [11,14]. The investigation of cation distribution in ferrites, between tetrahedral and octahedral sites, provides information about the various factors that determines the coordination preferences in structural chemistry. Some recent studies [15-17] have emphasized the need for understanding of the cation distribution of complex systems. Neutron diffraction is a very good procedure to understand the atomic structure and, in many cases, can give unambiguous picture of the cation distribution since neutron coherent scattering lengths of elements adjacent to each other in the periodic table may differ significantly [12,14,18-19]. In spinel, different physical and chemical properties are strongly dependent on the distribution of cations within the structure. In particular, the magnetization of the spinel systems strongly depends on the distribution of cations over the tetrahedral (A) and octahedral (B) sites. Recently, spinels are found to be good for electrode supports in solid oxide fuel cells [20-22]. In the present work, we have studied the crystal and magnetic structure of the spinel oxides $Zn_xCo_{1-x}Fe_2O_4$ (x=0.0, 0.25, 0.50 and 0.75)

International Conference on Mathematics, Engineering and Industrial Applications 2014 (ICoMEIA 2014)
AIP Conf. Proc. 1660, 090050-1–090050-10; doi: 10.1063/1.4926639

using X-ray and neutron diffraction techniques. In these spinels there are a large number of cations with different ionic sizes and their distribution over the A and B sites is of particular interest since the ferrimagnetic moment depends strongly on their cation distribution. Remanence magnetic moment, coercieve force and saturation magnetic moments have been measured to find the magnetic behavior.

EXPERIMENTAL

The spinel samples $Zn_xCo_{1-x}Fe_2O_4$ (x=0.0, 0.25, 0.50 and 0.75) have been prepared by traditional solid state sintering method. High purity (~99.9%) NiO, ZnO, CuO and Fe_2O_3 oxides were mixed thoroughly in exact stoichiometric ratios in a motar and pestle. The mixed powders were then ball milled for six hours in a stainless steel ball mill to produce fine powders. A small amount of distilled water was used as a milling fluid for fine mixing of the ingredients. Then the slurries were dried, palletized and transfer to a porcelain crucible for pre-firing at a temperature of 800°C for eight hours in air. After this pre-sintering operation, the pellets were again powdered, ball milled and re-palletized for final sintering at 1250°C for 6 hours. The X-ray diffraction experiments have been carried out in order to check the phases using the X-ray diffractometer ($CuK\alpha_1$, λ=1.54056Å) at the Atomic Energy Center, Dhaka, Bangladesh. The X-ray diffraction patterns recorded in the angular range $15°\leq 2\theta \leq 85°$ with a step size of 0.02º showed sharp peaks corresponding to a single phase spinel structure. The magnetization measurements on all the samples were carried out at room temperature using vibrating sample magnetometer (VSM) at the Atomic Energy Center, Dhaka, Bangladesh.

Neutron powder diffraction experiment was carried out at room temperature using the Triple Axis Neutron Spectrometer (TAS) at the 3MW TRIGA Mark II research reactor at AERE, Savar, Dhaka. Monochromatic neutrons beam of wavelength λ=1.236Å obtained by Bragg reflection from a Cu(200) monochromator. About 8 gms of powder samples were put in a cylindrical vanadium container of 8mm dia. The neutron flux at the sample position is approximately 10^5 neutron $cm^{-2}s^{-1}$. The neutron diffraction experiments were carried out in the angular range $10°\leq 2\theta \leq 90°$ with a step size of 0.2°.

The powder neutron diffraction data thus collected were analyzed using computer program FullProf [23] in the Rietveld method [17]. Rietveld refinement of the neutron diffraction data provides a precise determination of the crystal structure in terms of the positions, widths and intensities of the Bragg peaks. Peak shapes were quantified by a pseudo-Voigt function. Peak asymmetry correction was applied for reflections below 65^0 in 2θ. In the refinement process the background intensities were refined using a Chebyshev polynomial function with six coefficients. Each structural model was refined to convergence, with the best result selected on the basis of agreement factors and stability of the refinement. In the last cycle of the refinements, about 16 parameters were varied including scale factor, zero shift, peak shape parameter, half width, oxygen position parameters, lattice parameters, over all isotropic temperature factors and occupancies.

RESULTS AND DISCUSSION

The formation of single phase spinel structure for all the samples of the spinel system $Zn_xCo_{1-x}Fe_2O_4$ has been characterized by X-ray diffraction measurement. X-ray diffraction patterns showed sharp Bragg peaks corresponding to a cubic spinel structure with space group Fd3m. FIGURE 1 show the X-ray diffraction patterns for the spinel oxides $CoFe_2O_4$ and $Zn_{0.5}Co_{0.5}Fe_2O_4$ at room temperature. It is evident from the patterns that no impurity phase was found to exist for these samples.

Neutron diffraction measurements were performed at room temperature for the determination of the crystal and magnetic structure of the samples. FIGURE 2 shows the experimental neutron diffraction patterns for the samples $Zn_xCo_{1-x}Fe_2O_4$ (x=0.0, 0.25, 0.50 and 0.75) at room temperature. For the determination of correct magnetic structure it is essential to determine the exact cation distributions of the tetrahedral (A) and octahedral (B) sites of the spinel lattice. In spinel structures, both the crystallographic and magnetic unit cells are the same having identical symmetry relations. Therefore, the nuclear and magnetic contributions to the Bragg peaks occur at the same scattering position giving rise to an additional intensity in the diffraction patterns. But due to strong form factor dependence, the magnetic contributions rapidly fall off with scattering angle. Hence, the magnetic contributions are limited to the Bragg peaks in the low-Q region. Taking advantage of this, it is possible to determine the crystal and magnetic structure from the same neutron diffraction pattern. For the determination of the crystal structure we have considered only the higher angle neutron diffraction data where the magnetic contribution is negligible and for the magnetic

structure we have considered the total neutron diffraction data. For determining the cation distribution and other crystallographic parameters the higher angle ($43° \leq 2\theta \leq 90°$) neutron diffraction data, where magnetic contribution to the Bragg intensities is negligible, was profile analyzed using the computer program FullProf [23] in the Rietveld method [24].

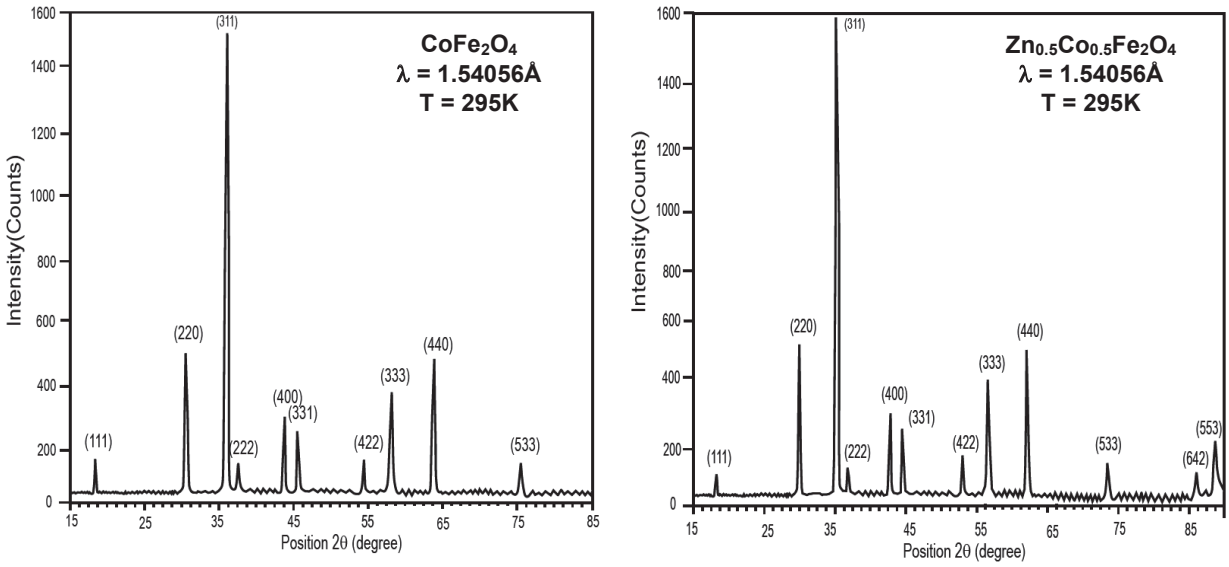

FIGURE 1. Indexed X-ray diffraction patterns for $CoFe_2O_4$ and $Zn_{0.5}Co_{0.5}Fe_2O_4$ in the cubic symmetry in Fd3m space group.

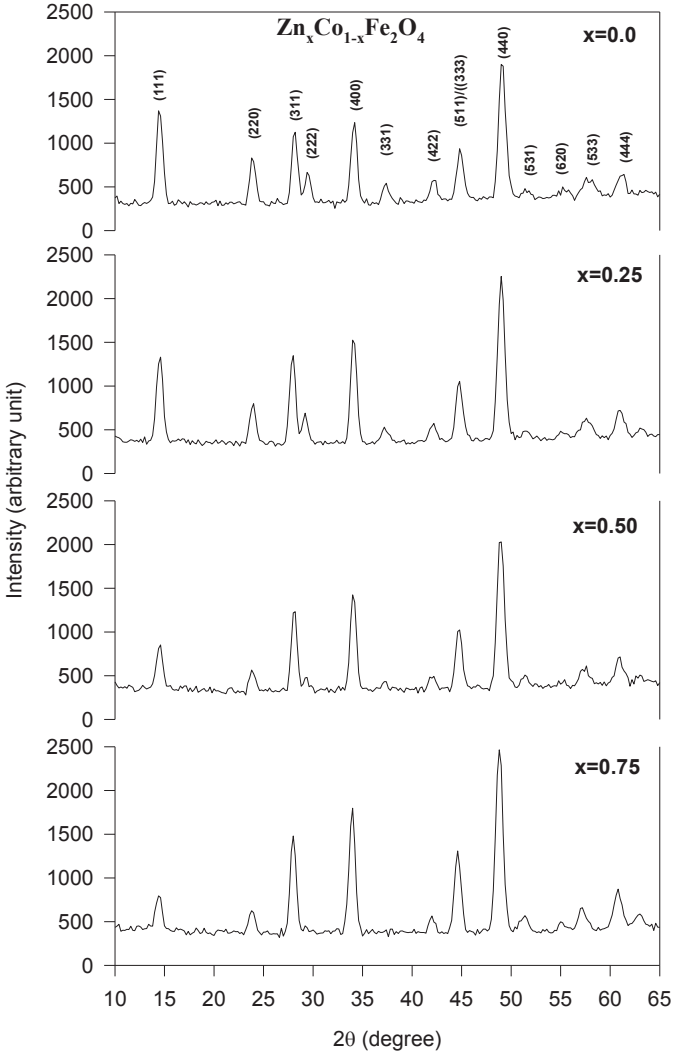

FIGURE 2. Neutron diffraction patterns of the spinel oxide $Zn_xCo_{1-x}Fe_2O_4$ (x=0.0, 0.25, 0.50 and 0.75) at room temperature. All the patterns were indexed in the cubic symmetry in the space group Fd3m.

The spinel structure has the symmetry of the space group Fd3m and this has been used in the data refinement for generating the calculated profile. The distributions of cations in tetrahedral (A) and octahedral (B) sites and other crystallographic parameters have been obtained from the Rietveld refinement of the room temperature neutron diffraction data. FIGURE 3 shows the fitted neutron diffraction pattern for the spinel oxides $Zn_{0.5}Co_{0.5}Fe_2O_4$ confined to the higher angle (above 40 deg 2θ) neutron diffraction data considering only nuclear contributions at higher angles. A very good agreement between the observed and calculated patterns is evident from the figure.

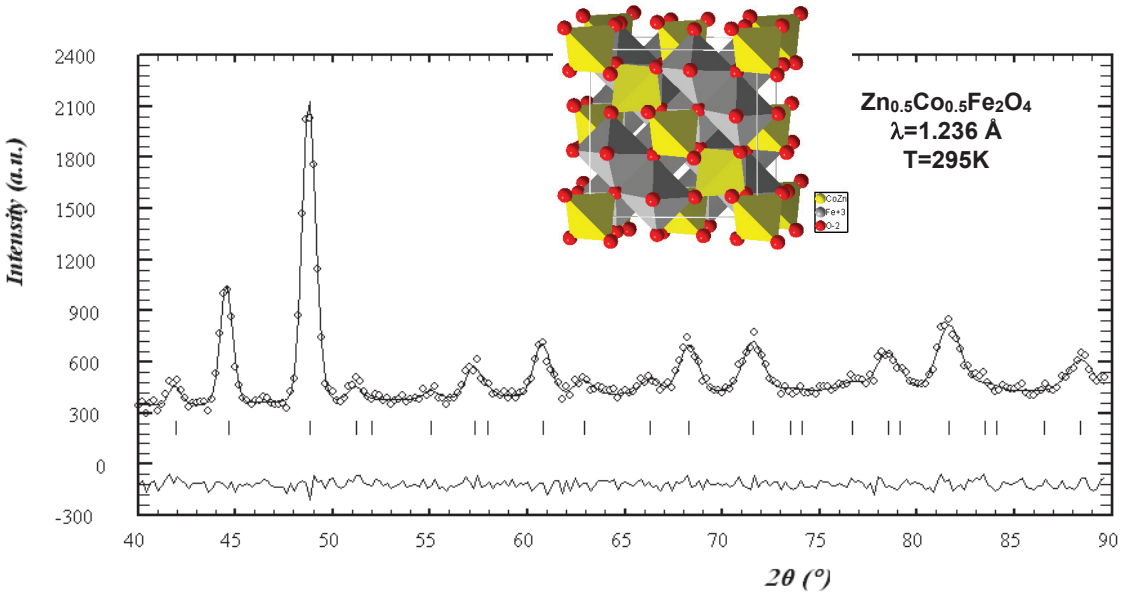

FIGURE 3. NPD Rietveld refinement intensity profiles for $Zn_{0.5}Co_{0.5}Fe_2O_4$ at room temperature considering only nuclear contributions. Observed (circles), calculated (continuous line) and the short vertical lines indicate the angular position of the allowed Bragg reflections. At the bottom in each figure the difference plot, I_{obs}-I_{calc}, is shown. Schematic 3D representation of the crystal structures are shown in inset. Co/Zn atoms are inside the tetrahedra (yellow), Fe atoms are inside octahedra (gray) and Oxygen atoms (ball, red) are situated in the corners of tetra and octahedra.

The values of cell parameters, overall temperature factor, oxygen position, refinement factors (R-factors) and χ^2 obtained from the Rietveld refinement of the neutron data in the nuclear phase are given in TABLE 1. The cell parameter and oxygen position parameter increases with increasing the Zn concentration in the system. This small increase in cell parameter with increasing x could be attributed to the slightly larger radius of the Zn^{2+} (~ 0.74 Å) which has been increasingly substituted for Co^{2+} (~ 0.75 Å) in the system. This small change in the unit cell dimensions does not show any appreciable change in the peak positions with increasing x, as shown in FIGURE 2. The oxygen position parameter lies within its normal limit of 0.25 and 0.27 for the spinel.

TABLE 1. Refined cell parameter, overall temperature factor, oxygen position parameter, R-factors and χ^2 of $Zn_xCo_{1-x}Fe_2O_4$ (x=0.0, 0.25, 0.50 and 0.75) obtained from NPD data at room temperature.

X	*a (Å)*	$B_{overall}$*(Å^2)*	*u (O)*	*R-factors (%)*
0.0	8.4236 ±0.0036	0.51 ±0.13	0.25656 ±0.00042	R_{Bragg}=5.69, R_F=4.39, R_P=3.95, R_{WP}=5.06, R_E=4.31, χ^2 = 1.38
0.25	8.4429 ±0.0030	0.74 ±0.10	0.25757 ±0.00042	R_{Bragg}=2.99, R_F=2.13, R_P=3.41, R_{WP}=4.29, R_E=4.20, χ^2 = 1.05
0.50	8.4570 ±0.0035	0.43 ±0.10	0.25870 ±0.00042	R_{Bragg}=3.76, R_F=3.99, R_P=3.96, R_{WP}=4.90, R_E=4.28, χ^2 = 1.31
0.75	8.4667 ±0.0029	0.36 ±0.08	0.26047 ±0.00032	R_{Bragg}=2.80, R_F=3.09, R_P=3.58, R_{WP}=4.65, R_E=4.08, χ^2 = 1.30

In complex spinels, the different cations are distributed over the A and B sites. The coherent scattering lengths of Co, Zn and Fe for neutrons are 2.49, 5.68 and 9.45fm, respectively. The significant difference in the coherent scattering lengths is advantageous and important for the correct determination of cation distribution. In the refinement process, initially Co was kept fixed on the B site since Co usually show this site preferences [18,25,26]. Then the occupancies of Zn and Fe on the two sites were varied within the stoichiometric constraint. Finally, the

occupancies of Co were varied separately one by one with Zn and Fe. The change in cation distribution in the structure upon Zn substitution obtained from the Rietveld refinement is listed in TABLE 2.

TABLE 2. Cation distribution from the Rietveld analysis of the NPD data for the spinel oxides $Zn_xCo_{1-x}Fe_2O_4$ at room temperature.

x	**Cation Distribution**	
	Tetrahedral or A site	Octahedral or B site
0.0	$(Co_{0.07}Fe_{0.93})_A$	$[Co_{0.93}Fe_{1.07}]_B$
0.25	$(Zn_{0.25}Co_{0.11}Fe_{0.64})_A$	$[Co_{0.64}Fe_{1.36}]_B$
0.50	$(Zn_{0.32}Co_{0.16}Fe_{0.52})_A$	$[Zn_{0.18}Co_{0.34}Fe_{1.48}]_B$
0.75	$(Zn_{0.62}Co_{0.12}Fe_{0.26})_A$	$[Zn_{0.13}Co_{0.13}Fe_{1.74}]_B$

The results revealed that for the sample $Zn_{0.25}Co_{0.75}Fe_2O_4$, Zn occupied only A-site. As the Zn concentration increased, Zn was found in both A and B site, where Zn concentration started with 9% for x = 0.5 and decrease to 6.5% for x = 0.75 at the B-site. At the A-site, Co concentration was increased and Fe concentration was found to be decreased for all compositions. At the B-site, Co concentration was decreased and Fe concentration was increased for all samples. FIGURE 4 shows a graphical representation of the site occupancies with Zn content.

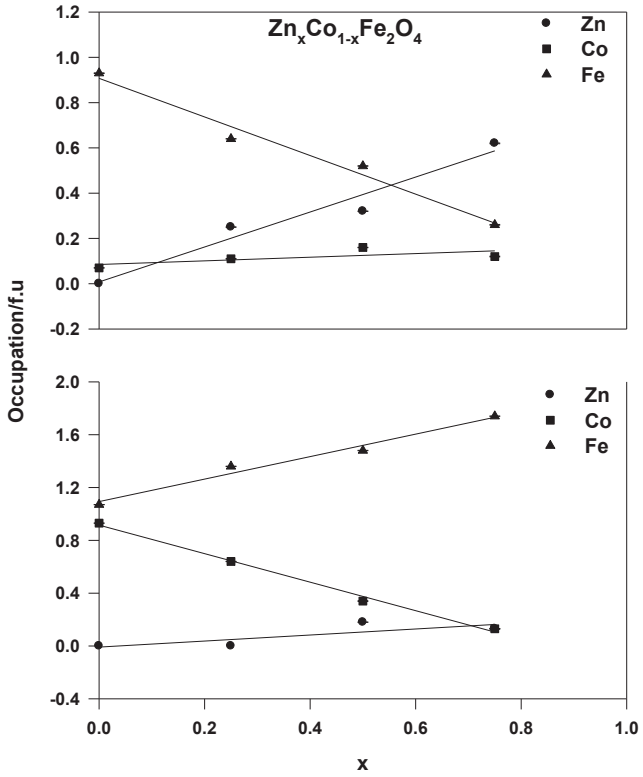

FIGURE 4. Plot of occupancy versus Zn-concentration in $Zn_xCo_{1-x}Fe_2O_4$.

Due to the cubic symmetry of nuclear and magnetic structure of spinel systems, the magnetic Bragg peaks override the nuclear Bragg peaks in the diffraction patterns. Therefore, the Bragg peaks in the neutron diffraction pattern contain both nuclear and magnetic information. Rietveld analysis of the total neutron diffraction data ($10°\leq 2\theta \leq 90°$) containing both nuclear and magnetic contributions were analyzed using the program FullProf [23] in two different phases. Both the nuclear phase and the magnetic phase crystallize in the cubic Fd3m space group. For

double phase refinement using Fullprof, the site occupancies of cations on both the tetrahedral and the octahedral sites were kept fixed as determined from the higher angle neutron diffraction data and other parameters were varied freely. The symmetry operators for the magnetic atoms were supplied as external input to the program. It was observed from the refinement process that the low angle Bragg peaks e.g. (111), (220), (222) possess large magnetic contributions.

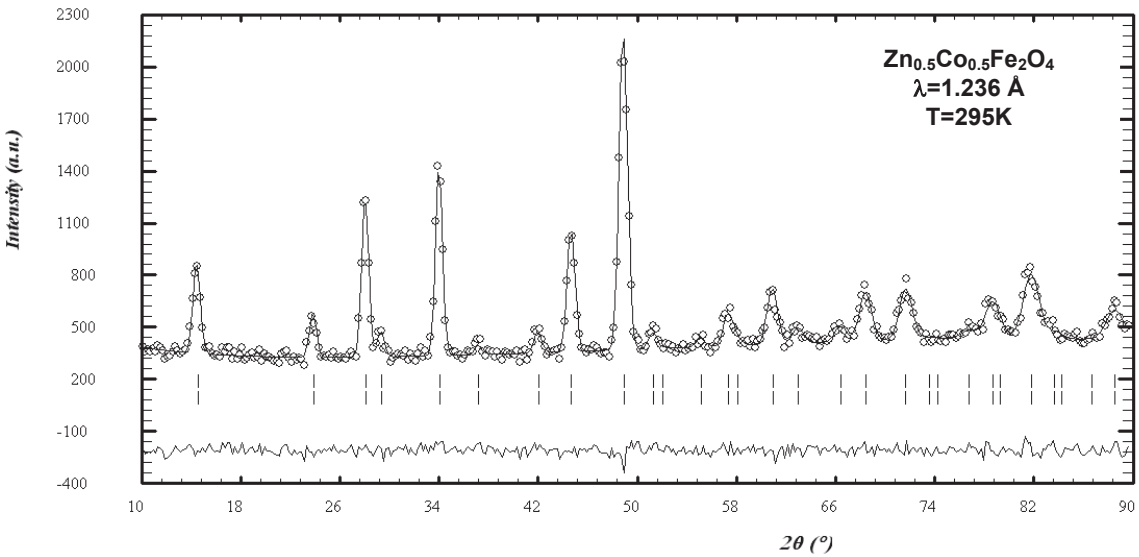

FIGURE 5. NPD Rietveld refinement intensity profiles for $Zn_{0.5}Co_{0.5}Fe_2O_4$ at room temperature considering both nuclear and magnetic contributions. Observed (circles), calculated (continuous line) and the short vertical lines indicate the angular position of the allowed Bragg reflections. At the bottom in each figure the difference plot, I_{obs}-I_{calc}, is shown.

FIGURE 5 show the plot of profile matching result of the Rietveld refinement of the total neutron diffraction data in the 2θ angular ranges 10–90° comprising both nuclear and magnetic contributions for the $Zn_{0.5}Co_{0.5}Fe_2O_4$ ferrite. It is evident from the figure that the agreement between the observed and calculated intensities is quite satisfactory. The sublattice and net magnetizations for all the compositions have been obtained from the Rietveld refinement of neutron data. FIGURE 6 shows the plots of sublattice and net magnetic moments as a function of Zn concentration. In spinel compounds the number of B sites are double the number of A sites. Thus the B site magnetization is usually larger than that of the A site and consequently the net moment being simply the difference between the two sublattice moments is normally parallel to the B sublattice moment [26]. A decreasing tendency of the strength of magnetization with increasing substitution of diamagnetic Zn ion in the system is quite evident from this plot. Net magnetic moment becomes zero for 75% Zn substitution of Co. All the samples under study have been found to possess ferrimagnetic ordering at room temperature.

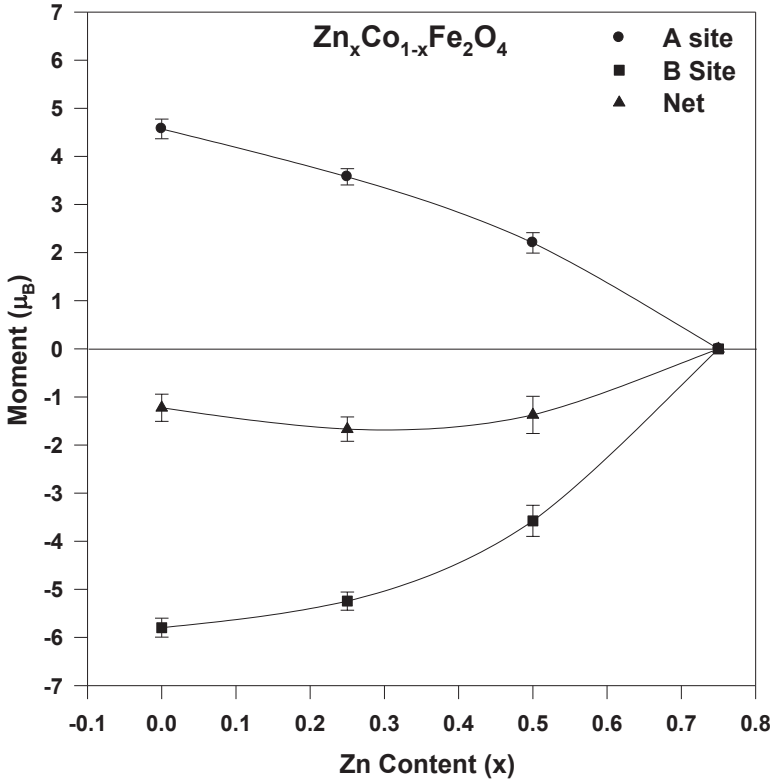

FIGURE 6. Variation of the sublattice and net magnetic moments with Zn concentration.

Remanence magnetic moments, coercieve forces and saturation magnetic moments were determined from the hysteresis curves obtained from the magnetization measurement of the samples. The values of the remanence magnetic moments, coercieve forces and saturation magnetic moments for different Zn (x values) substitutions are presented in TABLE 3. Remanence moment increases up to 50% Zn concentration and then decrease. Similarly, saturation magnetization increases up to 25% Zn concentration and then decreases. On the other hand, coercieve force decreases with Zn-concentration except for x = 0.75.

TABLE 3. Remanence magnetic moment, coercieve force and saturation magnetic moments for the spinel oxides $Zn_xCo_{1-x}Fe_2O_4$ at 295K.

x	Remanence magnetic moment, M_r (emu/g)	Coercieve force H_C (Oersted)	Saturation magnetic moment, M_S (emu/g)
0.0	21.07	341.82	76.49
0.25	39.91	111.47	91.80
0.50	59.63	34.99	74.29
0.75	0.114	58.47	5.21

The saturation magnetization as a function of Zn concentration is shown in Fig. 7. The saturation magnetization increases with increasing Zn concentration (x) in the initial stage with the optimum value of x estimated as 0.3 (Fig. 7). The saturation magnetic moment decreases with the further increase of x. This decrease is due to the decrease in magnetic AB interactions and as the colinearity of the sublattices are disturbed.

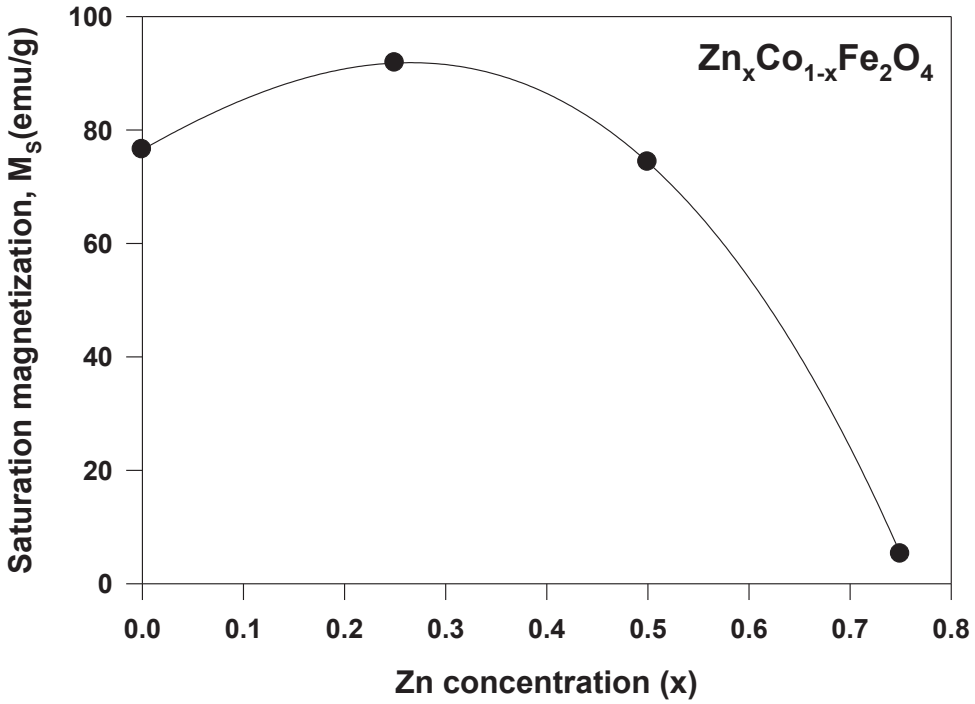

FIGURE 7. Dependence of saturation magnetization with Zn concentration.

CONCLUSIONS

Single-phase polycrystalline complex spinel samples of $Zn_xCo_{1-x}Fe_2O_4$ (x=0.0, 0.25, 0.50 and 0.75) were obtained by solid-state reaction and have been characterized by X-ray, neutron diffraction and magnetization measurements. All compositions crystallize in the cubic symmetry in the space group Fd3m. Neutron diffraction measurements gives a clear picture of structural parameters including cation distribution over A and B-site. The values of different crystallographic parameters and cation distributions are obtained in the best fit condition from the Rietveld analysis of the neutron diffraction data. The lattice constant increase with increasing the Zn content in the system. The magnetic structure was found to be ferrimagnetic for the samples with $x \leq 0.50$. Magnetization measurements show that with the increase of Zn content in the system the value of saturation magnetization first increases and then decreases. The variation of the magnetic moment with Zn substitution has been discussed in terms of the distribution of magnetic and non-magnetic ions over the A and B sub-lattices and their exchange coupling. Undoped sample show a small concentration of Co at the A-site but with Zn-doping Co concentration increases. The major occupation of Fe was found at the octahedral location which is a well-documented fact. The knowledge of this cation distribution is useful for determining the electrical and magnetic properties. For detailed magnetic behavior of the system the temperature dependent neutron diffraction study is needed.

ACKNOWLEDGMENTS

The authors are grateful to Bangladesh Atomic Energy commission for providing the neutron beam time for NPD experiments. They also grateful for the financial help from the SIDA/VR Sweden-Bangladesh project. AKA is thankful for the help and cooperation from Pg Dr. M. Iskandar, Dean, FIT, UBD.

REFERENCES

1. N. W. Grimes, *Phys.in Tech*. **22**, 6 (1975).
2. R. J. Hill, J. R. Craig and G. V. Gibbs, *Phys. Chem. Miner*. **4**, 317 (1979).
3. J. Kulikowski, *J. Magn. Magn. Mater*. **41**, 56 (1994).
4. A. Aslam, M.U. Islam, I. Ali, M.S. Awan, M. Irfan and A. Iftikhar, *Ceram. Inter.* **40**, 156-162 (2014).
5. K. Raju, G. Venkataiah and D.H. Yoon, *Ceram. Inter.* in press (2014). DOI: 10.1016/j.bbr.2011.03.031.
6. I. Ali, M.U. Islam, M.N. Ashiq, H.M. Khan, M.A. Iqbal and M.N.U. Haq, *Mater. Res. Bull*. **49**, 338 (2014).
7. X. Xu, A.K. Azad and J.T.S. Irvine, *Catalysis Today*, **199**, 22-26 (2013).
8. S. G. Algude, S. M. Patange, S. E. Sirsath, D. R. Mane and K. M. Jadhav, *J. Magn. Mag. Mater*. **350**, 39 (2014).
9. P. C. Pullar, W. Hajjaji, J. S. Amaral, M. P. Seabra and J. A. Labrincha, *Waste Bio. Valor*, **5**, 133 (2014).
10. N. Najmoddin, A. Beitollahi, H. Kavas, S. M. Mohseni, H. Rezaie, J. Akerman and M. S. Toprak, *Ceram. Int.* **40**, 3619 (2014).
11. A. K. Azad, S. G. Eriksson, S. M. Yunus, J. Eriksen and H. Rundlof, *Physica B* **327**, 1-8 (2003).
12. S. M. Yunus, A.K. Azad, S. G. Eriksson, J. Eriksen, H. Rundlof and R. Mathieu, *Physica B* **337**, 323-332 (2003).
13. A. K. M. Zakaria, M. A. Asgar, S. G. Eriksson, F. U. Ahmed, S. M. Yunus, A. K. Azad and H. Rundlof, *Mater. Lett.* **57**, 4243-4250 (2003).
14. G. A. Petptt, *Solid State Commun.* **13**, 1611 (1973).
15. S. M. Yunus, J. A. Fernandez-Baca, M. A. Asgar, F. U. Ahmed and M. A. Hakim, *Physica **B*** **262**, 112 (1999).
16. A. K. M. Zakaria, M. A. Asgar, S. -G. Eriksson, F. U. Ahmed, S. M. Yunus and M.A. Hakim, *AIP Conference Proceedings*, **1003**, 139 (2007).
17. M. A. Arillo, M. L. Lopez, M. T. Feernandez, M. L. Veiga and C. Pico, *J. Solid State Chem.* **125**, 211 (1996).
18. M. Laarj, S. Kacim and B. Gillot, *J. Solid State Chem.* **125**, 67 (1996).
19. T. Moriga, T. Sakamoto, Y. Sato, A.H. Khalid, R. Suenari and I. Nakabayashi, *J. Solid State Chem.* 1**42**, 206 (1999).
20. E. Stefan, P. A. Connor and J. T. S. Irvine, *J. Mater. Chem.* A **1,** 8262 (2013).
21. E. Stefan, G. Tsekouras and J. T. S. Irvine, *Adv. Ener. Mater.* **3,** 1454 (2013).
22. E. Stefan and J. T. S. Irvine, *J. Mater Sci.* **46,** 7191 (2011).
23. J. Rodrigues-Carvajal, *Physica B* **192**, 55 (1993).
24. H. M. Rietveld, *J. Appl. Crystallgr.* **2**, 65 (1969).
25. S. M. Yunus, H. –S. Shim, C. –H. Lee, M. A. Asgar, F. U. Ahmed and A. K. M. Zakaria, *J. Magn. Magn. Mater.* **241**, 40 (2002).
26. A. K. M. Zakaria, M. A. Asgar, S. -G. Eriksson, F. U. Ahmed, S. M. Yunus and H. Rundlof, *J. Magn. Magn. Mater.* **265**, 311-320 (2003).